Thermal and structural damping of the multiple-scattering contributions to the x-ray-absorption coefficient

M. Benfatto and C. R. Natoli
Laboratori Nazionali di Frascati, Istituto Nazionale di Fisica, Nucleare, Casella Postale 13, I-00044 Frascati, Italy

A. Filipponi
Consorzio per la Ricerca Scientifica e Tecnologica, Padriciano 99, I-34012 Trieste, Italy
and Dipartimento di Fisica, Prima Università degli Studi di Roma, La Sapienza, I-00185 Roma, Italy
(Received 27 June 1988; revised manuscript received 24 July 1989)

We present a method to calculate both the thermal and the structural damping of the multiple-scattering (MS) contributions to the x-ray-absorption coefficient. In the thermal case the correlation matrices between the coordinates of the atoms connected by MS paths are calculated, in the harmonic approximation, using the high-temperature expansion for the vibrational correlation function. When an additional structural disorder is present equivalent correlation matrices can be obtained from proposed models. These matrices define the widths of the corresponding Gaussian peaks in the n-body structural correlation functions. We present two different methods of calculation which can be generalized to non-Gaussian distributions: the first consists of a simple random sampling over the distribution of displacements, the second uses the Taylor expansion of the MS signal around the equilibrium position of the atoms in the path. The results are equivalent and indicate that only for χ_2 the dominant damping is given by a simple Debye-Waller-type correction in the amplitude. Both for the χ_3 and for the χ_4 signals, phase effects become important and can alter the effective damping. Implications on the convergence of the MS series will be discussed. In the case of structural disorder we show how the MS signal present in the x-ray-absorption spectra is capable of providing new structural information and will allow us to distinguish between various proposed models.

I. INTRODUCTION

The possibility that x-ray-absorption spectra might contain structural information beyond the pair correlation function probed by the single-scattering extended x-ray-absorption fine-structure (EXAFS) signal has been indicated by several authors.[1,2] In particular, Natoli and Benfatto have pointed out that under certain conditions the multiple-scattering (MS) series might be absolutely convergent, so that on general mathematical grounds they could predict three energy regions in an x-ray spectrum: a full-multiple-scattering region (FMS), generally (but not necessarily—it might even be missing as in a free-electron metal) at low energy, where many or an infinite number of MS paths of high order contribute to shape the absorption coefficient (depending on whether the series converges or not), followed by an intermediate-MS region (IMS), where only few paths of low order are relevant (typically single-, double-, and triple-scattering paths), with this latter region merging into a single-scattering region (SS) where only the EXAFS signal is important. Consequently, the existence of the IMS region is a necessary condition for obtaining information beyond the radial distribution function.

In this respect several applications to simple, test systems have led to encouraging results.[2–5] Detectable double-scattering signals have been shown to be in MnO_4^- ion in solution[2] and crystal silicon,[5] double and triple-scattering signatures in ferrocene,[3] and a triple-scattering contribution in $Cu(H_2O)_6^{2+}$ ion in solution.[3] In all these cases, however, the experimental analysis was limited by our inability to assess the effect of the configuration average with respect to the thermal spread of the atomic positions on the amplitude and phase of the MS signal. In fact a main point not yet clarified at the theoretical level is the effect of the thermal vibrations of the atoms on the various contributions to the MS series. The effect on the EXAFS is the well-known Debye-Waller factor.[6] The exact damping on the EXAFS contributions which takes also into account the exact spherical-wave phase effects has been calculated[7] and shows only very small corrections from the simple Debye-Waller term. The effect of the thermal vibrations on a general MS contribution is similarly expected to reduce the amplitude of the signal, and therefore it is an important phenomenon to be taken into account for its effects on the convergence of the MS series and for the quantitative analysis of the MS contributions. Moreover, in the case of highly disordered systems the configurational average is expected to modify substantially the shape of any MS signal, so that a calculation for fixed atom position is absolutely meaningless.

It is the aim of this paper to present a general method to calculate the damping of the MS contributions, taking into account, for the first time, both the correlation effects in thermal and structural disorder and the curva-

ture of the electronic propagators. This is performed in Sec. II. In Sec. III we report a numerical application to crystalline and amorphous silicon. In the latter case we show that, in principle, it is possible to distinguish between various proposed models for an amorphous structure by looking at the shape and intensity of the MS contributions. In another paper (referred to as Ref. 17 here) the application to the analysis of the k edge of amorphous silicon is given. Section IV is reserved for the conclusions.

II. THEORY

A. Damping of the MS signals

It has been shown[2] that any MS signal can be expressed in terms of two real (amplitude and phase) functions

$$\chi_n(k)=A(k,\mathbf{r})\sin[kR_p+\phi(k,\mathbf{r})] . \tag{1}$$

Here n is the number of segments (propagators) in the path, $\mathbf{r}$ is a set of coordinates describing the geometry of the n-segment path which can be selected among a wide choice of displacement coordinates, both Cartesian or curvilinear, like distances and angles, and k is the momentum of the photoelectron. Let $m \le n$ be the number of scatterers (including the origin) in the path. The minimum number of coordinates in three dimensions will be $3\times m-6$ for $m>2$ and 1 for $n=m=2$. Here we shall not specify the coordinate choice. R_p is the total path length which depends on $\mathbf{r}$. The amplitude $A(k,\mathbf{r})$ and the phase $\phi(k,\mathbf{r})$ are a cumbersome sum over angular momenta and their exact expressions will not be considered in this section. The important fact is that A, ϕ, and R_p depend on the geometry, i.e., on the displacements $\mathbf{r}$ from the equilibrium positions of the atoms.

Initially we will assume that the distribution of the generalized coordinates $\mathbf{r}$ is Gaussian, namely

$$P(\mathbf{r})d\mathbf{r}=\frac{e^{-(\mathbf{r},M^{-1}\mathbf{r})/2}}{(2\pi)^{N/2}\det[(M)^{1/2}]}d\mathbf{r} . \tag{2}$$

In the above and successive expressions the quantities $(\ldots)$ are quadratic forms. A Gaussian distribution is a very good approximation in the case of thermal broadening at low temperature. In the case of structural disorder, as we shall see, the Gaussian approximation is sufficient for the nearest coordination shells in a wide class of covalent materials. A generalization to non-Gaussian distribution is, however, possible.

The quantum statistical average of the MS contribution is the average over the distribution; that is,

$$\langle\chi_n(k)\rangle=\int d\mathbf{r}\frac{e^{-(\mathbf{r},M^{-1}\mathbf{r})/2}}{(2\pi)^{N/2}\det[(M)^{1/2}]}A(k,\mathbf{r}) \times\sin[kR_p+\phi(k,\mathbf{r})] . \tag{3}$$

For small displacements, a Taylor expansion truncated at some low order will be accurate enough. Therefore,

$$A(k,\mathbf{r})=A(k,0)+\nabla A(k,\mathbf{r})|_0\cdot\mathbf{r} +\tfrac{1}{2}(\mathbf{r},\mathsf{H}A(k,\mathbf{r})|_0\mathbf{r})+O(|\mathbf{r}|^3) , \tag{4a}$$

$$\phi(k,\mathbf{r})=\phi(k,0)+\nabla\phi(k,\mathbf{r})|_0\cdot\mathbf{r} +\tfrac{1}{2}(\mathbf{r},\mathsf{H}\phi(k,\mathbf{r})|_0\mathbf{r})+O(|\mathbf{r}|^3) , \tag{4b}$$

where H is the multidimensional second-derivative, or Hessian, operator. Now the total path length can be expanded in the same way:

$$R_p=R_p^{\mathrm{eq}}+\mathbf{v}\cdot\mathbf{r}+\tfrac{1}{2}(\mathbf{r},\mathsf{H}R_p|_0\mathbf{r})+O(|\mathbf{r}|^3) . \tag{5}$$

In a Cartesian-coordinate system the first-order term $\mathbf{v}$ is a vertical array formed by the vectors:

$$\nabla_{r_0,j}R_p|_{r=0}=\hat{\mathbf{v}}_j-\hat{\mathbf{v}}_{j+1} , \tag{6}$$

$\hat{\mathbf{v}}_j$ being the equilibrium versor of the jth segment in the path. Each of the vectors (6) is orthogonal to the bisector of the angle formed by the segments j and $j+1$ of the path. In the following we will introduce the total phase $\psi(k,\mathbf{r})=kR_p+\phi(k,\mathbf{r})$ and its Taylor expansion $\psi=\psi_0+\psi_1\cdot\mathbf{r}+\frac{1}{2}(\mathbf{r},\psi_2\mathbf{r})+\cdots$; also, the coefficients of the expansion for the amplitude will be indicated as A_0, A_1, and A_2.

The damped MS contribution, using the Taylor expansions, can be reduced to a series of Gaussian integrals:

$$\begin{aligned}\langle\chi_n(k)\rangle&=\mathcal{T}_m\int d\mathbf{r}\frac{e^{-(\mathbf{r},\mathsf{M}^{-1}\mathbf{r})/2}}{(2\pi)^{N/2}\det[(\mathsf{M})^{1/2}]}[A_0+A_1\cdot\mathbf{r}+\tfrac{1}{2}(\mathbf{r},A_2\mathbf{r})]\exp\{i[\psi_0+\psi_1\cdot\mathbf{r}+\tfrac{1}{2}(\mathbf{r},\psi_2\mathbf{r})]\}\\ &=\mathcal{T}_m\int d\mathbf{y}[A_0+i(A_1,\mathsf{Q}\psi_1)-\tfrac{1}{2}(\mathsf{Q}\psi_1,A_2\mathsf{Q}\psi_1)+(A_1+iA_2\mathsf{Q}\psi_1)\cdot\mathbf{y}+\tfrac{1}{2}(\mathbf{y},A_2\mathbf{y})]\\ &\quad\times\frac{e^{-(\mathbf{y},\mathsf{Q}^{-1}\mathbf{y})/2}}{(2\pi)^{N/2}\det[(\mathsf{M})^{1/2}]}e^{i\psi_0-(\psi_1,\mathsf{Q}\psi_1)/2} .\end{aligned} \tag{7}$$

Here Q is the complex matrix $(\mathsf{M}^{-1}-i\psi_2)^{-1}$ and $\mathbf{y}=\mathbf{r}-i\mathsf{Q}\psi_1$. After some simple algebraic manipulations and limiting ourselves to the first-order corrections, we obtain the following expression for the damped MS contribution, which turns out to be

$$\langle\chi_n(k)\rangle=A_0\left[1+\frac{(A_1,\mathsf{M}\psi_1)^2}{A_0^2}\right]^{1/2}e^{-(\psi_1,\mathsf{M}\psi_1)/2}\sin\left[kR_p+\phi_0+\frac{(A_1,\mathsf{M}\psi_1)}{A_0}\right] . \tag{8}$$

The dominant damping term is due to the exponential factor $e^{-(\psi_1,\mathsf{M}\psi_1)/2}$ which reduces to the usual Debye-Waller factor in the case of χ_2 and constant ϕ. The other corrections for the amplitude and the phase are of the order of A_1 and are expected to be small.

In the EXAFS case, the path will be described by a single coordinate: the displacement along the bond distance and the matrix M will be simply the bond-distance variance σ^2. The bond length R is counted twice in the path length; therefore the derivative of the total phase will be $\psi_1=2k+\nabla\phi$. Neglecting terms of the order of A_1 and $(\nabla\phi)^2$, we get

$$\langle\chi_2(k)\rangle = A_0 e^{-(2k^2+k\nabla\phi)\sigma^2}\sin(2kR+\phi_0)\ . \tag{9}$$

An analytic expression in terms of the atomic phase shifts for this EXAFS term will be derived in the Appendix.

In the general case the leading damping term is the exponential of $-\frac{1}{2}(kv+\nabla\phi,\mathsf{M}(kv+\nabla\phi))$ which contains both the contributions from the variation of the total path length and from the change of the phase induced by the change in the geometry. Now, the normal modes which contribute to the first effect are mainly "high-frequency" modes because they involve the stretching of near neighbors. These modes also contribute to the $\nabla\phi$ term, but the resulting effect is smaller. On the other hand, there are several "low-frequency" modes which contribute mainly to angle bending, which without affecting the total path length can considerably deform the path geometry and consequently produce changes in the ϕ term. These modes can provide, in general, an additional non-Debye-Waller–like damping, i.e., a damping not simply proportional to k^2.

We can understand an important conceptual difference which exists when going from single scattering to χ_3 and to $\chi_{n>3}$. In the first case these are no "low-frequency" modes, in the sense specified above, which can produce a large ϕ-induced damping, because the geometry of the path (segment) is rigid. As we go to χ_3 or even $\chi_{n>3}$, in the case of a nondegenerate path, these modes can have a considerable role in the damping of the signal.

We conclude that the $\nabla\phi$ term may give an important contribution to the damping of the $\chi_{n\geq 3}$ terms of the MS expansion. We also observe that the term $\nabla\phi$ does not generally give rise to a Debye-Waller–like damping and consequently it could be effective even at small **k** values, the region in which the convergence problems are more critical.

B. Generalized non-Gaussian distribution

The generalization of the previous treatment to non-Gaussian distributions is performed as follows. We expand the signal to first order in both amplitude and phase. For a generalized displacement distribution $P(\mathbf{r})$ we write

$$\langle\chi_n(k)\rangle = \mathcal{T}_m\int d\mathbf{r}\,P(\mathbf{r})A_0\exp[i(\psi_0+\psi_1\cdot\mathbf{r})] + \mathcal{T}_m\int d\mathbf{r}\,P(\mathbf{r})(\mathbf{r},A_1)\exp[i(\psi_0+\psi_1\cdot\mathbf{r})]\ . \tag{10}$$

This can be easily written in terms of the characteristic function of the probability distribution:

$$\Phi_c(\mathbf{t}) = \int d\mathbf{r}\exp(i\mathbf{r}\cdot\mathbf{t})P(\mathbf{r})\ . \tag{11}$$

We obtain

$$\langle\chi_n(k)\rangle = \mathcal{T}_m\left[A_0\exp(i\psi_0)\Phi_c(\psi_1) - i\exp(i\psi_0)\left[\frac{d}{d\psi_1},A_1\right]\Phi_c(\psi_1)\right]\ . \tag{12}$$

Now, writing the characteristic function by means of the multidimensional cumulant expansion,[8] using the usual convention on the repeated indexes, we have

$$\Phi_c(\mathbf{t}) = \exp\left[-\tfrac{1}{2}t^it^jK_2^{i,j} - i\frac{1}{3!}t^it^jt^kK_3^{i,j,k} + \frac{1}{4!}t^it^jt^kt^lK_4^{i,j,k,l} + \cdots\right]\ . \tag{13}$$

We get

$$\begin{aligned}\langle\chi_n(k)\rangle &= \mathcal{T}_m\exp(i\psi_0)\Phi_c(\psi_1)\{A_0 + i[A_1^iK_2^{i,j}\psi_1^j + (i/2)A_1^iK_3^{i,j,k}\psi_1^j\psi_1^k - \tfrac{1}{6}A_1^iK_4^{i,j,k,l}\psi_1^i\psi_1^k\psi_1^l + \cdots]\}\\ &\approx \{[A_0 - \tfrac{1}{2}(A_1^iK_3^{i,j,k}\psi_1^j\psi_1^k)]^2 + [(A_1^iK_2^{i,j}\psi_1^j) - (1/3!)(A_1^iK_4^{i,j,k,l}\psi_1^j\psi_1^k\psi_1^l)]^2\}^{1/2}\\ &\quad\times\exp[-\tfrac{1}{2}(\psi_1^iK_2^{i,j}\psi_1^j) + (1/4!)(\psi_1^iK_4^{i,j,k,l}\psi_1^j\psi_1^k\psi_1^l)]\\ &\quad\times\sin\left[kR_p+\phi_0-\frac{1}{3!}(\psi_1^iK_3^{i,j,k}\psi_1^j\psi_1^k) + \frac{(A_1^iK_2^{i,j}\psi_1^j) - \frac{1}{3!}(A_1^iK_4^{i,j,k,l}\psi_1^j\psi_1^k\psi_1^l)}{A_0 - \frac{1}{2}(A_1^iK_3^{i,j,k}\psi_1^j\psi_1^k)}\right]\ .\end{aligned} \tag{14}$$

We observe that in the case of a Gaussian distribution K_2 is M, all the other cumulants are null, and we correctly obtain, as a limit, the previous result of Eq. (8). The expression describes appropriately the damping expected in the case of nonsymmetric distributions, where a non-Debye-Waller–like damping and a phase shift are expected. We observe that, in order to perform the calculation, only the derivative of the amplitude and the phase are again needed. Only the description of the probability distribution becomes more complex.

C. Thermal correlation matrices for path displacements

In a previous paper[9] one of us has presented the method of the high-temperature expansion (HTE) for the calculation of the vibrational correlation function (VCF) in the harmonic approximation. The possible application to calculate the thermal damping of the MS signals was mentioned. In this subsection we outline this last application in some detail.

For a general harmonic system described by a kinetic matrix T and a potential matrix V it is possible to obtain the high-temperature expansion for the VCF in the form

$$\langle q_i q_j \rangle = \frac{1}{\beta}\left[V^{-1}+\frac{(\beta\hbar)^2}{12}T^{-1}-\frac{(\beta\hbar)^4}{720}[T^{-1}(VT^{-1})] + \cdots + \frac{B_{2n}(\beta\hbar)^{2n}}{(2n)!}[T^{-1}(VT^{-1})^{n-1}]\right]_{ij}, \tag{15}$$

where β is the usual Boltzmann factor. The matrix VCF contains all the correlations between any set of Lagrangian coordinates $\{q_i\}$ and consequently defines the thermal width of any peak of any n-body structural correlation function: $g_2(r)$, $g_3(r_1,r_2,r_3)$, ... In this regard we must emphasize that this is certainly one of the main characteristics of the HTE method. Some authors have used the method of the continued-fraction expansion for the diagonal elements of the Green's[10] function to calculate mean-square relative displacements (MSRD's) of bulk and surfaces in crystals.[11] This method requires the calculations of the density of states, which is redundant information in our context. Here the calculation of the 21 elements needed for a χ_4 is simply performed at one time, inverting the whole potential matrix in the HTE method.

Let us assume we have a set of $d\times(N-1)$ relative coordinates. Let us further assume we are interested in calculating the damping of an n-atom MS path starting from the atom 0 to 1,2, . . . , $n-1$,0. The geometry of the path would be univocally determined by $3\times n-6$ coordinates in three dimensions. Now there are several possible choices for the coordinates: they can be Cartesian or curvilinear according to convenience. Sometimes it may be easier to use a number larger than the minimal one; for instance, it is possible to use $3\times n-3$ coordinates without taking into account the rotational invariance of the path. In our thermal calculations, however, we used a minimal set of relative Cartesian displacements in which the first atom in the path lies always in the x-axis direction and the second on the x-y plane. The generic Cartesian component will be indicated as $r_{0,j}$, $j=(1,2,\ldots,3n-6)$, and using a compact notation the whole vector will be indicated as $\mathbf{r}$. This set of relative coordinates can be expressed as a linear combination of Lagrangian coordinates, namely

$$r_{0,j}=\sum_l S_{j,l}q_l \quad \text{or} \quad \mathbf{r}=S\mathbf{q}\ . \tag{16}$$

The correlation matrix between the set of $r_{0,j}$ can indeed be calculated in a straightforward manner from the VCF:

$$\mathsf{M}=\langle r_{0,i}r_{0,j}\rangle=\sum_{l,k} S_{i,l}\langle q_l q_k\rangle S_{j,k}$$

or

$$\mathsf{M}=\langle \mathbf{r}\mathbf{r}^+\rangle=S\langle \mathbf{q}\mathbf{q}^+\rangle S^+\ . \tag{17}$$

This correlation matrix defines the shape of the $(3\times n-6)$-dimensional Gaussian peak in the n-body structural correlation function caused by the n-segment path previously considered, given by Eq. (2).

The practical example that we will consider is the prototype case of c-Si. In this case the VCF was calculated with the method presented in Ref. 9 using a Keating potential and clusters of up to 238 atoms. The values for the force constants used in such calculations were $\alpha=145.5$ N/m and $\beta/\alpha=0.16$. The results for the MSRD's of the first 12 shells are reported in Table I for the temperatures 80, 300, and 500 K.

We also considered representative paths for higher-order contributions to the MS series. The choice was made among the major signals which contribute to the shape of the photoabsorption spectrum. In Fig. 1 we sketch the local order around a central atom (labeled 0) where the paths are displayed by arrows. We selected a 3-segment path joining the atoms 0-1-2-0, belonging to the first and second coordination shells of the crystal, and

TABLE I. MSRD's of the first 12 shells in c-Si at 80, 300, and 500 K.

Shell	Atoms	Neighbor	Distance (Å)	MSRD (10^{-3} Å^{-2}) 80 K	300 K	500 K
I	4	1	2.3520	2.622	3.400	4.748
II	12	2	3.8408	4.24	7.95	12.29
III	12	3	4.5037	4.80	9.83	15.43
IV	6	4	5.4317	5.00	10.54	16.61
V	12	3	5.9191	4.56	8.96	13.98
VI	24	4	6.6525	4.89	10.13	15.93
VII	16	5	7.0560	5.04	10.65	16.90
VIII	12	4	7.6816	4.79	10.00	15.37
IX	24	5	8.0336	4.98	10.48	16.50
X	24	6	8.5883	5.31	11.23	18.42
XI	12	5	8.9045	4.94	10.44	16.31
XII	8	6	9.4080	5.01	10.62	16.74

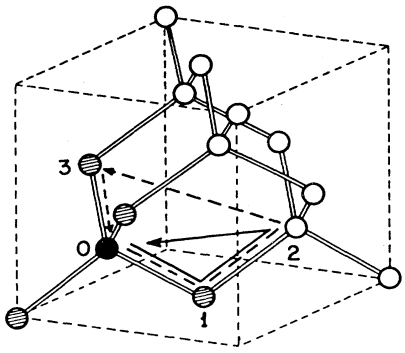

FIG. 1. Local order of the c-Si structure. The χ_3 path 0-1-2-0 and the χ_4 path 0-1-2-3-0 are shown by the arrows.

the 4-segment path 0-1-2-3-0 which returns to the atom 0 through a further first-shell atom (labeled 3) in a staggered position with respect to atom 2. In Table II we report as an example the correlation matrices M between the six Cartesian relative displacements which describe the atom vibrations of the whole 4-segment path. Obviously the upper left 1×1 block, displayed by the first dotted line, is the first-shell MSRD. The upper left 3×3 block, on the other hand, is the correlation matrix for the 3-segment path 0-1-2-0.

D. Structural correlation matrices in disordered solids

We shall focus our attention on a particular class of disordered solids: the amorphous covalent solids and, in particular, amorphous silicon (a-Si). This was chosen because we wanted to show in an explicit case the new information which can be gained by accurate data analysis of a disordered system. On the other hand, the methods which are presented here are very general and can be applied to other classes of materials.

Amorphous covalent solids are characterized by a strong nearest-neighbor bond with a well-defined length plus a slightly weaker bond angle determined by the hybridization of the valence shell. For these reasons the radial distribution function resembles that of the crystalline counterpart up to the second coordination shell. For instance, in a-Si the first shell has an additional structural contribution to the variance of the bond length which is only of the same order of magnitude as the thermal one at room temperature. The structural contribution for the second shell peaks exactly at the crystalline value although it is broadened by a structural contribution approximately 1 order of magnitude larger than the thermal one. Starting from the third shell, the dihedral-angle freedom distributes the neighbors over a wide range of distances, washing out other relevant peaks in the $g_2(r)$.

Theoretical radial distribution functions can be obtained from available models of a-Si systems. Since Polk's pioneering ball-and-stick model,[12] sophisticated computer algorithms have been developed. Starting from an empirical potential, one can perform, by means of a switching-bond procedure, a Monte Carlo simulation of the disordered network as in the Wooten-Winer-Weaire[13] (WWW) model, or directly perform a molecular-dynamics calculation as in the recent Biswas-Grest-Soukoulis[14] (BGS) model. The final structure will depend both on the potential model used and on additional constraints (i.e., four-fold coordination for the WWW model) included in the procedure. Inspection of the models will provide information on the static n-body correlation functions. From this analysis it is possible to distinguish the overlapping contributions from different neighbors. For instance, it is possible to separate second neighbors from third neighbors in the near-eclipsed position and realize that the distribution of the former is very close to a Gaussian shape, a fact that cannot be proven experimentally because the two distributions overlap.

An analysis of the models at a level of higher-order correlation functions has never been performed before the present work. g_3 is the distribution of the triangles joining atom sites and can be expressed as a function of any choice of three numbers which define the form of the triangles. Just like g_2, g_3 will be composed of a few well-defined peaks, as far as first or second neighbors are involved, which merge into a diffuse uniform distribution as the distances increase. In order to calculate the ex-

TABLE II. Vibrational correlation matrix, at 300 K, in units of 10^{-3} Å^2 referring to the χ_4 which joins the atoms 0-1-2-3-0 of Fig. 1. The equilibrium coordinates of the atoms in Å are 0, (0.000,0.000,0.000); 1, (2.352,0.000,0.000); 2, (3.136,2.217,0.000); 3, (−0.784,1.108,1.920). The six rows and columns in the matrix refer, from the top downward and from the left to the right, to the displacement of atom 1 along the x direction, the displacement of atom 2 on the x-y plane, and the displacement of atom 3 along x, y, and z. Because of the rotational invariance the axes are defined such that atom 1 always lies on the x axis and atom 2 on the x-y plane. The X_1,X_1 term is obviously the first-shell MSRD, while the upper-left 3×3 block is the vibrational correlation matrix for the χ_3 path 0-1-2-0.

	X_1	X_2	Y_2	X_3	Y_3	Z_3
X_1	3.400	2.004	0.214	1.397	0.107	0.186
X_2	2.004	17.50	−5.939	7.696	5.931	−0.172
Y_2	0.214	−5.939	6.067	−2.603	−2.337	0.128
X_3	1.397	7.696	−2.603	16.88	−1.447	7.941
Y_3	0.107	5.931	−2.337	−1.446	19.88	−10.07
Z_3	0.186	−0.172	0.128	7.941	−10.07	13.09

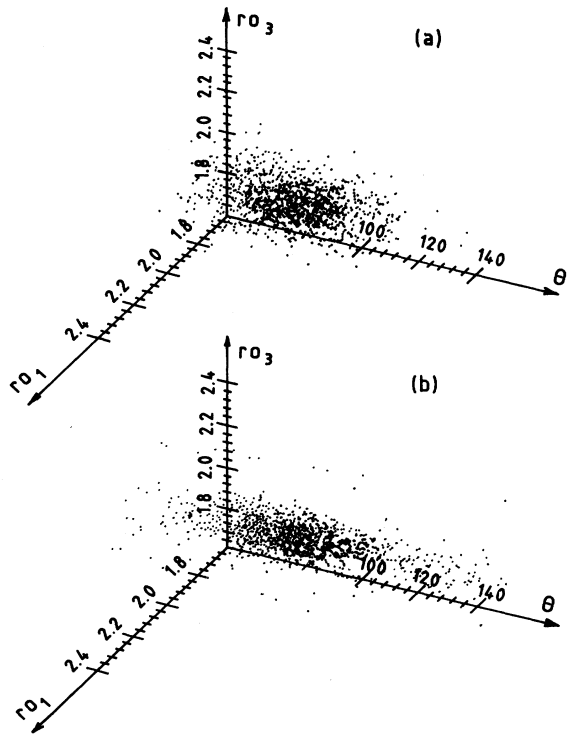

FIG. 2. Three-dimensional views of the fundamental peak of the three-body correlation function for the (a) Wooten-Winer-Wearie model and for the (b) Biswas-Soukoulis-Grest model. The peak refers to the basic triangle in the tetrahedron. The coordinates are, respectively, $r0_1$, the first bond length; θ, the angle between the two bonds 0-1 and 0-3; and $r0_3$ is, the second bond length (see Fig. 1). The peaks are evidently Gaussians and are centered around the c-Si values of 2.352 Å for the distances and 109.47° for the angle. The difference between the two models is evident.

pected contributions arising from χ_3 paths, we shall consider in this subsection the shape of the peaks of g_3 due to the basic triangle in the tetrahedron. We shall use as coordinates the two first-shell bond distances and the angle in between, whose average value should be the tetrahedral value of 109.47°; this choice will be justified later. The same distribution, $g_3(r_1,r_2,\theta)$, is useful for two different kinds of χ_3 signals: the path, which will be called χ_{3A}, within the tetrahedron (say 0-1-3-0 in Fig. 1, not indicated with the arrows), and the already considered path χ_{3B}, which also involves the second shell (the 0-1-2-0 in Fig. 1) and other χ_4 signals as discussed in detail in Ref. 15.

We computed the distribution of triangles for the following a-Si or a-Si:H models: (1) the Henderson model[16]; (2) the Guttman-Fong a-Si:H model[17]; (3) the Wooten-Winer-Weaire (WWW) model[13]; and (4) the Biswas-Grest-Soukoulis (BGS) model.[14]

As an example we report in Fig. 2 a three-dimensional view of $g_3(r_1,r_2,\theta)$ of the most recent models: the WWW model in Fig. 2(a) and the BGS model in Fig. 2(b). We note first that in such a coordinate choice the triangles' distribution can be satisfactorily expressed by a Gaussian. This is the proof that the Gaussian approximation for the structural disorder is not meaningless, and also that the present choice for the coordinates is appropriate. In Cartesian coordinates the points are distributed along the arc of a circle described by the angle fluctuations and further terms in $K_3^{i,j,k}$ should be considered.

A further fact we would like to stress is that the two models, which are among the most sophisticated available for a-Si, present large differences in the correlation functions.

Because of the Gaussian shape of the g_3 peaks and the identity of the two nearest-neighbor bonds, the distributions are completely defined by the average bond distance R and angle θ and four more parameters for the covariance matrix M, namely the bond-length ($\sigma_R=\sqrt{\mathsf{M}_{R,R}}$) and angle ($\sigma_\theta=\sqrt{\mathsf{M}_{\theta,\theta}}$) standard deviations and the bond-bond ($\rho_{R,R}=\mathsf{M}_{R1,R2}/\sigma_R^2$) and bond-angle [$\rho_{R,\theta}=\mathsf{M}_{R,\theta}/(\sigma_R\times\sigma_\theta)$] correlations. These two parameters are the additional information present in the g_3 peak that is not contained in g_2. In Table III we report the values for the four models considered. We see again that the differences are large; besides the σ values, the correlations also differ from model to model by a large amount, indicating, for instance, that in the BGS (molecular-dynamics) model bond-length fluctuations are less correlated to both adjacent bond and angle fluctuations than in the WWW or other models.

III. NUMERICAL CALCULATIONS

A. Computational methods

We used two different numerical methods of calculation of the damping effect. The first consisted in evaluating the integral in (3) generating a large number of paths, sampling in a random way the known Gaussian distribution of displacements and adding the resulting contributions. While it is obvious that this is not the most clever procedure, it must be considered that it is a safe method, which can be generalized to the case of non-Gaussian dis-

TABLE III. Parameters for the first peak of the three-body correlation function in various models for a-Si and a-Si:H.

Model	R (Å)	θ (deg)	σ_R (Å)	σ_θ (deg)	$\rho_{R,R}$	$\rho_{R,\theta}$
Henderson	2.348	109.2	0.089	12.3	0.072	0.184
Guttman and Fong	2.341	109.4	0.074	12.0	0.344	0.108
Wooten, Winer, and Weaire	2.354	109.2	0.060	11.3	0.313	0.145
Biswas, Grest, and Soukoulis	2.329	108.7	0.048	15.1	0.202	0.048

tributions, or which can be used directly on a given structural model. It turned out that a good sampling of the tails of the distribution is needed; otherwise the results are incorrect, especially at large k values. A reasonable size for the random sampling for a χ_3 distribution is 1000. This can be done in approximately 3 h of CPU time on a VAX 8650. In the case of wide distributions typical of the amorphous materials a larger sampling is needed. The application of this procedure to χ_4 turned out to be impossible since the time needed for the calculation of each χ_4 contribution is ≈ 3 min.

The second method consists of calculating numerically the gradients of the amplitude and the phase of the MS contribution and successively calculating the damping factor using Eq. (8) of the previous section. This second method was considerably faster and suitable for general use. However, the results are consistent only if the order, to which the Taylor expansion of the signal is truncated, is sufficient. In the calculations that we have performed we monitored the consistence of the results using both methods. First, the random sampling was used, increasing the size of the sampling, up to the convergence of both the actual covariance matrix and calculated spectrum, after a calculation with the derivative method was performed. The two methods give identical results, as has been verified both for thermal and structural disorder. From this we conclude that the first-order Taylor expansion of phase and amplitude is sufficient for our purposes.

B. Calculation for the thermal disorder in *c*-Si

We calculated the χ_2 signal due to the second coordination shell and the signals χ_3 and χ_4 due to the multiple-scattering paths previously described at the temperatures of 80, 300, and 500 K. In Fig. 3 we report the comparison between the undamped signals and the damped signals at 500 K for the three contributions. We observe that the χ_2 and χ_3 oscillate almost in opposition of phase; as already pointed out,[5] as a consequence, the effect of the thermal damping is particularly important to determine the shape of the total signal.

In order to compare the effective damping at the various temperatures we report in Fig. 4 the logarithm of the ratio of the damped amplitudes with the undamped amplitudes versus k^2 for the three signals (solid lines). The dotted lines represent the damping coming from the fluctuation of the total path length only, neglecting all the phase corrections ($\psi_1 = A_1 = 0$): the so-called "geometrical" contribution. These are easily calculated with the machinery of the HTE for the VCF. In a pure Debye-Waller–like case these plots should look like straight lines through the origin with a slope of $-2\sigma_p^2$, σ_p^2 being an equivalent MSRD for the path which actually is $\frac{1}{4}$ times the variance of the vibrational displacement of the total path length R_p. In the case of the χ_2 signals the damping is very close to the geometrical one, indicating that the phase effects are negligible. This result seems to be a general situation in agreement with the exact calculation of Ref. 7 and with the approximate treatment

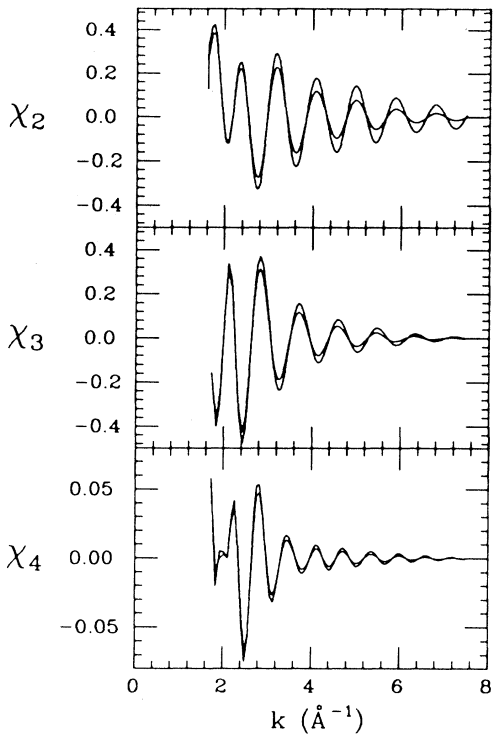

FIG. 3. Comparison between typical undamped multiple-scattering signals and their thermal averages at 500 K. From the top to the bottom the signals refer to the second-shell EXAFS or path 0-2-0 (χ_2), the double-scattering 0-1-2-0 (χ_3), and the triple-scattering 0-1-2-3-0 (χ_4), as shown in Fig. 1.

given in the Appendix. On the other hand, in the χ_3 and χ_4 cases the global behavior of the damping is different from the simply geometrical one as shown in Fig. 4 by the evident departure of the solid lines (which give the total damping) from the dotted lines. This is due to the effect of the $\nabla\phi$ term. Nevertheless, looking at the energy region between 10 and 50 Å^{-2}, it is possible to make a linear fit of the solid lines in order to extract approximately an effective MSRD (i.e., σ_p^2) for the studied MS contributions. In our case the results so obtained are about 20% more than the geometrical values for all the paths.

For comparison, these results are reported in Table IV together with the values of the geometrical MSRD. We would like to emphasize that in this case the real damping for $\chi_{n>2}$ is surprisingly smaller than the second-shell MSRD which damps the χ_2 signal. An explanation of this nonevident behavior lies in the fact that in the χ_3 considered the strongly vibrating second-shell bond is counted only once, while the same bond enters twice (with a total contribution of 4 in the MRSD) in the second shell, χ_2.

C. Calculations for the structural disorder in *a*-Si

In this subsection we report the results obtained for the two models of amorphous silicon: WWW and BGS. We

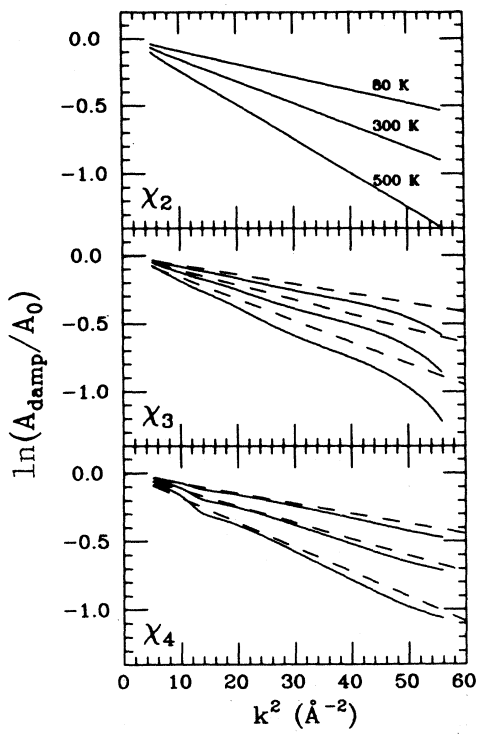

FIG. 4. Effective dampings for the three prototypical multiple-scattering, χ_2, χ_3, and χ_4, paths described in the text. On the y axis we report the logarithm of the ratio between damped and undamped amplitudes and on the x axis the square of the photoelectron momentum. In each plot three curves are reported which refer to the temperatures of 80, 300, and 500 K, as indicated in the plot for χ_2. The dashed lines refer to the pure geometrical damping, while the solid lines refer to the total effective damping which also takes into account the phase term.

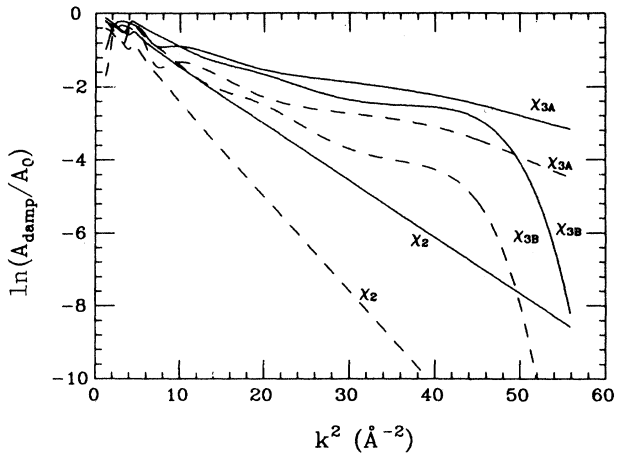

FIG. 5. Effective dampings for the three relevant multiple-scattering paths in the a-Si structure besides the trivial first-shell EXAFS. They are the second-shell χ_2 signal and the χ_{3A} and χ_{3B} double-scattering signals as described in the text. On the y axis we report the logarithm of the ratio between damped and undamped amplitudes and on the x axis the square of the photoelectron momentum. The solid lines refer to the Wooten-Winer-Weaire model, while the dashed lines refer to the Biswas-Soukoulis-Grest model. The difference between the corresponding signals is evident.

have calculated the second-shell χ_2 signal and the χ_{3A} and χ_{3B} signals previously described in Sec. II D. The reason for considering these contributions is that they contribute to the fine details besides the trivial first-shell EXAFS in the a-Si photoabsorption spectrum. The contribution from the χ_4 path considered for the c-Si case is, for instance, strongly washed out by the continuous dihedral-angle distribution.

In Fig. 5 we report the logarithm of the ratio of the damped to the undamped amplitudes for the three signals for the WWW model (solid lines) and for the BGS model (dotted lines). In this amorphous case the larger width of the Gaussian distribution resulted in larger damping of the signal, and in a very slight distortion due to the $\nabla\phi$ term also in the χ_2 case. Moreover, contrary to the thermal case, the phase effects in the χ_3 are very important. It is no longer possible to approximate the damping with a linear fitting and, at the same time, the term $(A_1, M\psi_1)/A_0$ in Eq. (8) becomes relevant, producing a dephasing between damped and undamped signals. This fact makes a phenomenological damping of Debye-Waller type in highly disordered cases completely meaningless. We also observe how the damping for the two χ_3 signals is considerably different even though their geometrical damping is identical (same triangle). This effect is totally due to differences in the phase contribution.

As clearly shown by Fig. 5, the two models give really different signals. The main effect is due to the larger angular spread in the BGS model than in the WWW model; however, there are other differences. If the two sets of lines were scaled to make the two χ_2 dampings coincide, the χ_3 damping lines would still not coincide. This effect

TABLE IV. Effective DW factor for several multiple-scattering paths at 300 K in c-Si. The geometrical contribution is reported for comparison. The total values refer to a linear fit in the region 10–50 Å^{-2}.

Path	Path length (Å)	Degeneracy	Effective MSRD at 300 K (10^{-3} Å^{-2}) Geometrical	Total
χ_2 0-2-0	7.682	12	8.08	7.99
χ_3 0-1-2-0	8.545	24	5.35	6.38
χ_4 0-1-2-3-0	11.56	48	6.03	6.46

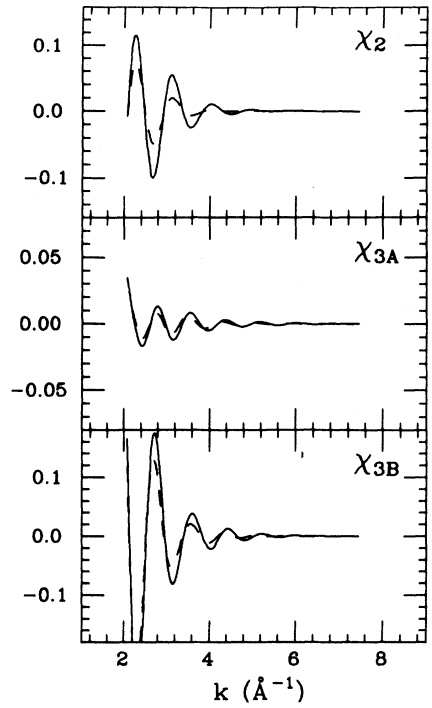

FIG. 6. Comparison of the signals χ_2, χ_{3A}, and χ_{3B} between the WWW and BGS models for a-Si. The differences in amplitude and in phase are evident. The dashed line refers to the BGS model.

must be also attributed to the difference in the correlation, which is the new information contained in g_3, as already pointed out in Table III.

In Fig. 6 we report, for completeness, the comparison between the mentioned signals calculated for the two models (the solid line refers to the WWW model). As expected, the signals show differences both in amplitude and in phase. The magnitude of these differences is well beyond the usual noise level in x-ray-absorption spectra. In order to make a real comparison with an experimental signal, a complete analysis of all MS paths and a good treatment of the inelastic losses in the solid medium should be performed. This work is presented in a subsequent paper, Ref. 15, where the x-ray-absorption spectrum of a-Si materials is interpreted in terms of single- and multiple-scattering contributions configurationally averaged on the basis of the present theoretical approach.

These results suggest that additional information beyond the radial distribution function can actually be obtained by means of a multiple-scattering analysis of the experimental signal and can open the way to the use of the x-ray-absorption spectroscopy as a means for understanding the local order in amorphous systems and discriminating among different models for amorphous structures.

IV. CONCLUSIONS

In this paper we have presented the theory of the vibrational and structural damping of the general term of the MS series. The importance of our formalism, conceptually easy to understand, lies in the fact that for the first time the correlations effects are included in the calculation. They are in the matrices M. Numerical results on the thermal effects in crystalline silicon and on the structural effects in amorphous silicon have been reported as protoypical cases. Nevertheless, our method is quite general and can be applied to other cases.

We have shown that the main vibrational damping is due to the geometrical Debye-Waller factor only for the χ_2 terms. On the contrary, phase corrections become important in the χ_3 or χ_4 terms and account for a large percentage of the total damping.

As a result of our analysis it is now clear that the general belief that the vibrational damping is stronger in $\chi_{n\geq 3}$ than in a single scattering signal is not well founded. In fact, we have presented an explicit case in which χ_3 has a smaller effective damping than χ_2. This is not a peculiarity of the systems considered; its origin lies in the low correlation present in the displacements of adjacent bonds compared to the total correlation present in the same bond which is counted twice in a general single-scattering path.

The application of our method of analysis to investigate structural disorder, using two recent models for amorphous silicon, has led to interesting results. The larger damping makes in this latter case χ_2 and χ_3 comparable in amplitude in such a way that the total signal turns out to be very sensitive to the differences in the structure, providing a way for discriminating different models of disorder. The experimental application of our method to the analysis of the K edge of amorphous silicon is given in Ref. 15. This research allows for the use of x-ray-absorption spectroscopy as a probe of higher-order correlation functions in various kinds of condensed systems.

ACKNOWLEDGMENTS

We would like to thank Dr. R. Biswas and Dr. K. Winer for providing us the coordinates of their computer models for amorphous silicon. One of us (A.F.) would like to thank the Synchrotron Radiation Center (University of Wisconsin–Madison) at Stoughton, WI for the hospitality given in the period during which most of this work was done.

APPENDIX

In this appendix we derive an analytic expression in terms of the atomic phase shifts for the damped EXAFS signal using, for the spherical-wave propagators[1] between sites i and j, the simple approximation

$$G^{ij}_{LL'}=4\pi Y_L(\hat{\mathbf{R}}_{ij})Y^*_{L'}(\hat{\mathbf{R}}_{ij})\frac{e^{i\rho_{ij}}}{\rho_{ij}}f_{ll'}(\rho_{ij}) ,$$

where $\rho=kR$, $L\equiv(l,m)$ is a collective angular-momentum index, and

$$f_{ll'}(\rho)=\left[1+\frac{\alpha_{ll'}}{2\rho^2}\right]^{1/2} e^{i\alpha_{ll'}/2\rho} .$$

Here $\alpha_{ll'}=l(l+1)+l'(l'+1)$. This simple approximation reproduces quite well the exact EXAFS term both in amplitude and phase. Following the same procedure used by Beni and Platzman,[6] it is easy to obtain an expression for curved EXAFS which accounts quite well for the Debye-Waller factor. The final result is

$$\langle\chi_2(k)\rangle=(-1)^l\mathrm{Im}\left\{\frac{e^{2i(\rho_j+\delta_l^0)}}{\rho_j^2}\sum_{l'}(-1)^{l'}(2l'+1)e^{i\delta_{l'}^j}\sin\delta_{l'}^j\left[e^{-\sigma_j^2\beta_{ll'}^2(k)/2}\left[1+\frac{\alpha_{ll'}}{2\rho_j^2}\right]e^{i\alpha_{ll'}/\rho_j}\right]\right\},$$

where l is the angular momentum of the final state, σ_j is the usual MSRD of the jth atom, and

$$\beta_{ll'}(k)=2k-\alpha_{ll'}/kR_j^2 .$$

Different calculated cases, which have not been reported here, are in agreement with the calculations described in the main text both in amplitude and phase behavior.

[1]C. R. Natoli and M. Benfatto, J. Phys. (Paris) Colloq. **47**, C8-11 (1986); P. J. Durham, J. B. Pendry, and C. H. Hodges, Solid State Commun. **38**, 159 (1981).

[2]M. Benfatto, C. R. Natoli, A. Bianconi, J. Garcia, A. Marcelli, M. Fanfoni, and I. Davoli, Phys. Rev. B **34**, 5774 (1986).

[3]M. F. Riuz-Lopez, M. Loos, J. Goulon, M. Benfatto, and C. R. Natoli, Chem. Phys. **121**, 419 (1988); G. Garcia, M. Sanchez del Rio, E. Burattini, M. Benfatto, and C. R. Natoli, Physica B+C **158B**, 409 (1989).

[4]M. Benfatto and C. R. Natoli, J. Non-Cryst. Solids **95&96**, 319 (1987).

[5]A. Bianconi, A. Di Cicco, N. V. Pavel, M. Benfatto, A. Marcelli, C. R. Natoli, P. Pianetta, and J. Woicik, Phys. Rev. B **36**, 6426 (1987).

[6]G. Beni and P. M. Platzman, Phys. Rev. B **14**, 1514 (1976); E. Sevillano, H. Meuth, and J. J. Rehr, *ibid.* **20**, 4908 (1979); E. A. Stern, B. A. Bunker, and S. M. Heald, *ibid.* **21**, 5521 (1980).

[7]C. Brouder (private communication).

[8]R. Kubo, J. Phys. Soc. Jpn. **17**, 1100 (1962).

[9]A. Filipponi, Phys. Rev. B **37**, 7027 (1988).

[10]V. Heine, R. Haydock, and M. J. Kelly, in *Solid State Physics*, edited by H. Ehrenreich, F. Seitz, and D. Turnbull (Academic, New York, 1980), Vol. 35.

[11]G. Tréglia and M. C. Desjonquères, J. Phys. (Paris) **46**, 987 (1985); M. C. Desjonquères and G. Tréglia, Phys. Rev. B **34**, 6662 (1986).

[12]D. E. Polk, J. Non-Cryst. Solids **5**, 365 (1971).

[13]F. Wooten, I. Winer, and D. Weaire, Phys. Rev. Lett. **54**, 1392 (1985).

[14]R. Biswas, G. S. Grest, and C. M. Soukoulis, Phys. Rev. B **36**, 7437 (1987).

[15]A. Filipponi, F. Evangelisti, M. Benfatto, S. Mobilio, and C. R. Natoli, following paper, Phys. Rev. B **40**, 9636 (1989).

[16]D. Henderson, J. Non-Cryst. Solids **16**, 317 (1974).

[17]L. Guttman and C. Y. Fong, Phys. Rev. B **26**, 6756 (1982).